Biomimetic microfluidic platform for the quantification of transient endothelial monolayer permeability and therapeutic transport under mimicked cancerous conditions

Christopher George Uhl,[1] Vladimir R. Muzykantov,[2] and Yaling Liu[1,3,a)]
[1]*Department of Bioengineering, Lehigh University, Bethlehem, Pennsylvania 18015, USA*
[2]*Department of Pharmacology, University of Pennsylvania, Philadelphia, Pennsylvania 19104, USA*
[3]*Department of Mechanical Engineering and Mechanics, Lehigh University, Bethlehem, Pennsylvania 18015, USA*

(Received 15 August 2017; accepted 14 December 2017; published online 2 January 2018)

Therapeutic delivery from microvasculature to cancerous sites is influenced by many factors including endothelial permeability, vascular flow rates/pressures, cancer secretion of cytokines and permeabilizing agents, and characteristics of the chosen therapeutics. This work uses bi-layer microfluidics capable of studying dye and therapeutic transport from a simulated vessel to a cancerous region while allowing for direct visualization and quantification of endothelial permeability. 2.5 to 13 times greater dye transport was observed when utilizing small dye sizes (FITC) when compared to larger molecules (FITC-Dextran 4 kDa and FITC-Dextran 70 kDa), respectively. The use of lower flow rates/pressures is shown to improve dye transport by factors ranging from 2.5 to 5 times, which result from increased dye diffusion times within the system. Furthermore, subjecting confluent endothelial monolayers to cancerous cells resulted in increased levels of vascular permeability. Situations of cancer induced increases in vascular permeability are shown to facilitate enhanced dye transport when compared to non-diseased endothelial monolayers. Subsequent introduction of paclitaxel or doxorubicin into the system was shown to kill cancerous cells resulting in the recovery of endothelial confluency overtime. The response of endothelial cells to paclitaxel and doxorubicin is quantified to understand the direct influence of anti-cancer therapeutics on endothelial growth and permeability. Introduction of therapeutics into the system showed the recovery of endothelial confluency and dye transport back to conditions experienced prior to cancer cell introduction after 120 h of continuous treatment. Overall, the system has been utilized to show that therapeutic transport to cancerous sites depends on the size of the chosen therapeutic, the flow rate/pressure established within the vasculature, and the degree of cancer induced endothelial permeability. In addition, treatment of the cancerous region has been demonstrated with anti-cancer therapeutics, which are shown to influence vascular permeability in direct (therapeutics themselves) and indirect (death of cancer cells) manners. Lastly, the system presented in this work is believed to function as a versatile testing platform for future anti-cancer therapeutic testing and development. *Published by AIP Publishing.* https://doi.org/10.1063/1.5000377

I. INTRODUCTION

The presence of diseased regions near vasculature can lead to states of increased endothelial monolayer permeability.[1–5] These increases in vasculature permeability are often the result

a)Author to whom correspondence should be addressed: yal310@lehigh.edu

of vascular permeabilizing agent production and excretion from diseased regions, such as cancerous regions.[1,3–5] In the case of cancerous regions, tumor benefits from increased vascular permeability include an improved supply of nutrients and removal of cellular waste products, as well as access to the vascular system allowing easy metastasis.[6–8]

In order to combat such diseased conditions, therapeutic delivery via the vascular system is often utilized.[7–11] However, this approach for delivering drugs can be difficult due to varying degrees of endothelial permeability and differences in pressure between the vasculature and the diseased site.[6,9,10,12–15] For the case of cancer, fluctuations in capillary level endothelial permeability occur as cancerous cells are killed off by anti-cancer drugs, resulting in an overall decrease in the production of vascular permeabilizing agents.[16,17] In turn, this allows for the vasculature to begin to repair and reduce permeability.[16,17] As further cancerous cells are targeted and killed, the degree of vascular permeability further reduces, in turn reducing the overall free transport of anti-cancer therapeutics.[16,17]

In addition to fluctuations in endothelial permeability, the occurrence of pressure differentials between blood vessels and diseased sites can also greatly influence therapeutic delivery.[13–15] Situations when vascular pressure is lower than that of the diseased region causes added difficulty when attempting to deliver therapeutics.[10,13–15] Examples from literature where interstitial fluid pressure is greater than vascular pressure leads to difficulties in delivering therapeutics to solid tumor sites and inflamed pulpal cells.[18,19] As such, understanding how differences in pressures and flow rates can influence the transport and delivery of therapeutics is beneficial for disease treatment.

In order to better understand the role of the endothelial barrier and the effect of cancerous cells on the transport of therapeutics to diseased regions, a bi-layer microfluidic device has been fabricated which allows for the co-culture of healthy endothelial cells with a secondary cell type.[20,21] This is achieved while also providing a means of control over the pressures generated in both layers of the device. Throughout the following work, physiologically relevant flow conditions are established in the mimicked vasculature while cancerous cells are used to create a tumor microenvironment. The presence of the cancerous cells provides the system with permeabilizing agents which act to modulate endothelial confluency. The application of flow induced pressures and the application of therapeutics provides insight into optimal treatment options for patient specific disease conditions.

As in any model, the physiological relevance of specific parameters varies. For example, a rather unconventional approach has been utilized to manipulate pressures within the system in a controlled manner. The pros and contras of this and other features of the model are carefully evaluated in the Discussion with consideration given to the data provided by the model.

Overall, this work has been geared around better understanding how the transient nature of the endothelial barrier, presence of flow derived pressures, and variations in system conditions influence the transport and delivery of therapeutics. Through this work, we aim to quantify tumor cell induced permeability of microvessels within a mimetic microfluidic system. In addition, we aim to quantify the temporal effect of therapeutics on the measured microvessel permeability throughout time-course treatments.

II. RESULTS

A. Microfluidic device production

Bi-layer microfluidic devices were produced and sterilized using an autoclave in order to permit culturing of both bovine aortic endothelial cells (BAOECs) and human colorectal cancer cells (HCT116s). Device integrity was suitable to allow for the flow of media, dyes, and therapeutics without leakage through the use of syringe pumps. A device schema can be observed in Fig. 1 which depicts the device layout and locations within the device where the BAOEC and HCT116 cells are grown for experimental testing. Full schemes depicting all device setups and testing conditions can be observed in supplementary material, Figs. SF 1 and SF 2. Physiologically relevant factors such as the presence of HCT116 cancer cells in close proximity to the vasculature and the natural production/excretion of permeabilizing agents were possible

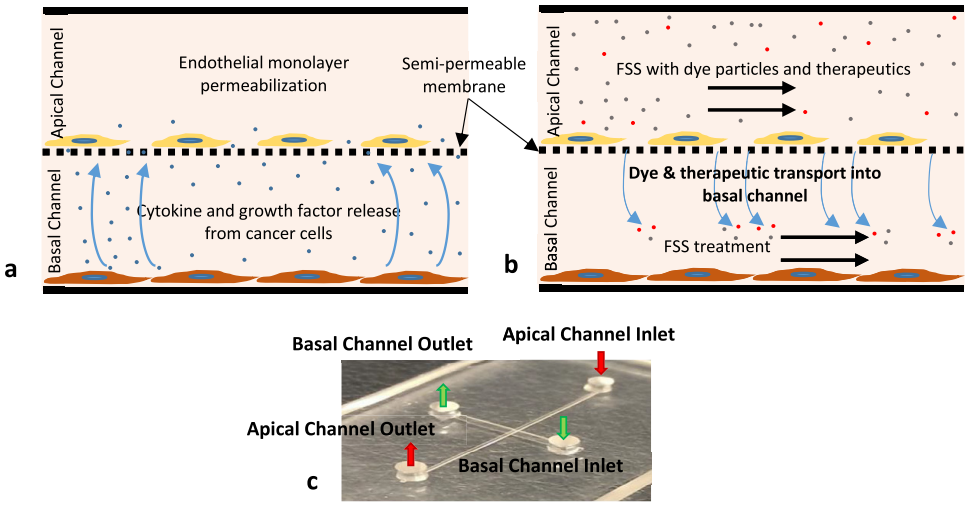

FIG. 1. Device schema depicting the culturing setup and experimental conditions for dye and therapeutic transport to the cancer region in the basal channel. (a) Bi-layer microfluidic device setup with the apical and basal channel separated by the semi-permeable membrane. A BAOEC endothelial monolayer is grown on the surface of the semi-permeable membrane and a HCT116 cancer monolayer is grown in the basal channel. Cytokines and growth factors released by the HCT116s influence the permeability of the BAOEC monolayer. (b) Device setup depicting therapeutic and dye transport across the permeabilized BAOEC monolayer and semi-permeable membrane in order to function on the HCT116s present in the basal channel. (c) Image of bi-layer device showing the apical and basal channel along with respective inlets and outlets.

utilizing the microfluidic setup.[5,22–24] However, it is recognized that for some factors, especially the oncotic pressures, the total range, and method utilized to achieve the desired goals are not physiologically relevant or accurate.[19,22,24] For this study a wide range of pressures, including extremes, were coupled with the use of shear derived pressure on the side of the cancerous region. Such experimental conditions were established in order testing the total capabilities of the system while providing the greatest amount of control over the system as a whole. The use of more physiologically relevant pressure ranges and use of protein concentration gradients to drive the pressure differences in the system would be more realistic.[19,25,26]

B. Cell confluency measurements

Cell confluency was measured using a plasma membrane (PM) stain, fluorescence imaging and confocal microscopy throughout time-course treatments with anti-cancer therapeutics. From the scans and images collected, the degree of cell monolayer coverage was measured as the area covered by cells expressed as a percentage of the whole viewing area. When only BAOECs were cultured within the devices the cell coverage was determined to be 97.5%. However, when HCT116s were introduced and grown in the basal channel, the degree of cell monolayer confluency dropped to 67.8%. Subsequent treatment of the diseased condition resulted in a steady increase in cell area coverage over the course of 120 h, back to similar conditions prior to introduction of the HCT116s. These changes in cell area coverage throughout Paclitaxel [Fig. 2(a)] and Doxorubicin [Fig. 2(b)] treatment can be seen in Fig. 2.

Complementary data were collected from confocal scans where conditions without HCT116s grown in the devices resulted in a low gap coverage of 2.8%. However, when HCT116s were introduced into the channels, the gap coverage increased to 37.9% as can be seen in supplementary material, Fig. SF 3. Both testing conditions and methods of data collection produced similar results indicating that the technique for quantifying the degree of BAOEC monolayer permeability functions well.

Representative images of typical results experienced under conditions when only BAOECs were grown in the device, as well as typical results experienced under conditions when BAOECs and HCT116s were grown in the device can be seen in Figs. 2(c) and 2(d), respectively, along with the supplementary material, Fig. SF 4. Figure 2(c) clearly shows a highly

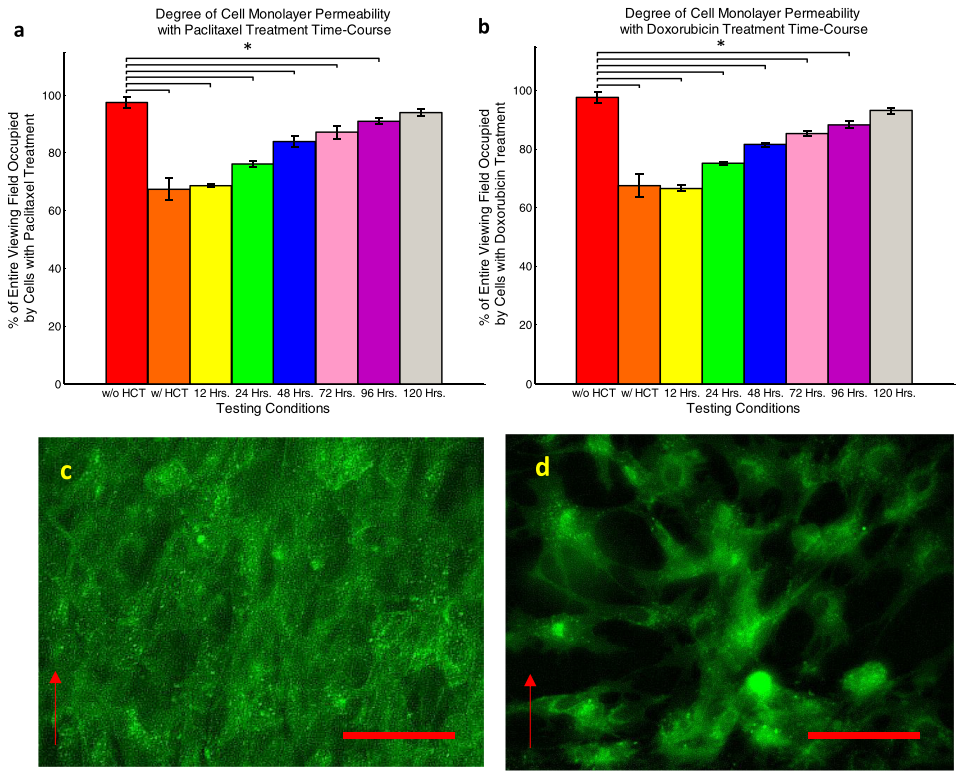

FIG. 2. Normalized percentage of BAOEC monolayer permeability under various culturing conditions. Data shown as a sum of means ± S.D. (n = 5 independent microfluidic devices) for each image collection method. (a) Percentage of confluent BAOEC monolayer intact without HCT116s, with HCT116s, after treatment with Paclitaxel, and after treatment with Doxorubicin for 24 h, measured as a percentage of the entire imaging field, collected via standard fluorescent microscopy. One way analysis of variance (one-way ANOVA) statistical analysis with statistical significance indicated by * brackets in plot at $p \leq 0.05$. Sample collection was carried out from 5 independent devices (biological replicates). All statistical tests have been justified as appropriate. (b) Percentage of intercellular gap coverage without HCT116s, with HCT116s, after treatment with Paclitaxel, and after treatment with Doxorubicin, measured as a percentage of the entire imaging field, collected via fluorescent confocal microscopy. One way ANOVA statistical analysis with statistical significance indicated by * brackets in plot at $p \leq 0.05$. Sample collection was carried out from 5 independent devices (biological replicates). All statistical tests have been justified as appropriate. (c) Representative fluorescent image of the highly confluent BAOEC monolayer prior to introduction of HCT116s into the device. Cells in the image were stained with Cell Tracker Green and the red arrow indicates the direction of flow within the channel. (**d**) Representative fluorescent image of the permeabilized BAOEC monolayer after introduction of HCT116s into the device. Cells in image were stained with Cell Tracker Green and the red arrow indicates the direction of flow within the channel. Both red scale bars are 50 μm in length.

confluent monolayer of BAOECs aligned with the direction of flow indicated by the red arrow. Dark spots between cells indicate that gaps are present in very low numbers and are small in size. Conversely, Fig. 2(d) shows sparsely spaced BAOECs with large dark gaps present between individual cells. In addition to standard fluorescence microscopy, representative confocal scans of highly permeabilized BAOEC monolayers were obtained and can be observed in the supplementary material, Fig. SF 5. Verification of the effect of paclitaxel and doxorubicin on the HCT116 cancer cells utilized in the study can be observed in the supplementary material, Fig. SF 11, where application of either anti-cancer drug resulted in HCT116 death over time. Additionally, the effect of paclitaxel and doxorubicin on BAOECs was verified over time. BAOECs were grown within microfluidic channels and subjected to culture media shear flow ($200\,s^{-1}$) containing anti-cancer therapeutics. The concentrations of the therapeutics used and the durations of the flow tests were held constant with all other testing. The presence of the anti-cancer therapeutics was shown to influence the survival and confluency of BAOECs grown within microfluidic devices. Treatment of the BAOECs occurred over the course of 120 h without the presence of any cancer cells in order to quantify the effect of the therapeutics on endothelial

cells. The resulting data indicated a slight increase in cell count over the first 24 h of treatment with the therapeutics. Further treatment of the endothelial cells (EC) with therapeutics over the full 120 h resulted in slight reductions of the cell counts. ECs treated over the same 120 h timeframe with standard culture media displayed improved growth which slowed over time as the ECs become more and more confluent within the devices. Likewise, when analyzing the coverage area of the EC monolayers as percentages over the time-course treatments, an initial increase was observed over the first 24 h followed by a reduction in the percentage of the area covered. The data and representative images relating to the BAOECs response to anti-cancer therapeutics can be observed in the supplementary material, Fig. SF 6.

C. Dye transport under equal flow rates and pressures

Bi-layer microfluidic devices were utilized to track dye transport from the apical channel into the basal channel under various experimental conditions. The specific dyes used in these studies were FITC, FITC-Dextran 4 kDa, and FITC-Dextran 70 kDa, chosen for their increasing size and molecular weight in order to mimic various small and large molecule therapeutic candidates. Additionally channel flow rates of 9190, 70150, and 253050 μl/h which correspond to average channel pressures of 632.8, 4832.4, and 17431.2 Pascals (Pa), respectively, were chosen to investigate the influence of a wide range of flow/pressure on therapeutic transport. The following figures contained in Fig. 3 plot out the normalized dye transport averaged across all testing conditions, using the confluent BAOEC monolayer testing conditions as a baseline (set equal to 1). All of the dye transport data collected has additionally been normalized to account for any loss of dye due to binding with channel walls or cells.

Figure 3(a) depicts the averaged dye transport achieved based on varying dye sizes. The data points represented in the figure are the average values from all tests run at various pressures and under various device conditions. The figure shows that on average, across all other testing conditions, the smallest FITC dye underwent the greatest degree of transport across the EC monolayer. Subsequently, the FITC-Dextran 4 kDa and FITC-Dextran 70 kDa dyes underwent less transport, respectively. This trend based on the dye size was observed for equal pressure testing due to diffusion which acts as the main driving factor for transport when no pressure gradient exists across the membrane. The amount of dye in each flow test was held constant and due to its small size, the FITC dye was able to undergo the greatest diffusion and subsequent transport when compared to the two larger dyes. Next, we turn our focus onto the influence of established pressures on the overall transport observed.

Figure 3(b) depicts the averaged and normalized dye transport achieved under various pressures established within the channels. It should be noted that no pressure gradient exists across the semi-permeable membranes in this work. As such, the pressures within both the apical and basal channels are changed equally to ensure no flow driven transport of dye occurs. When comparing the degree of dye transport, it is shown that the lowest pressure established resulted in the greatest amount of dye transport across all dye sizes and device conditions. Generally, the trend shows that increasing pressures within the channels results in lower transport regardless of dye size. The reason why this trend is observed is again due to the fact that the total amount of dye introduced during each test was held constant. As such, the total duration of the higher pressure flows was shorter when compared to the lower pressure tests due to the manner in which pressure is established in each channel. The shorter period of flow for the higher pressure cases results in less time for the dyes to undergo diffusion which ultimately results in less overall transport. If all established pressures for each dye test were given equal flow durations through the channels, the observed difference in transport would not be present, as demonstrated in the supplementary material, Fig. SF 10. Lastly for the equal pressure tests, the degree of dye transport achieved under various device conditions was examined.

Figure 3(c) depicts the normalized transport achieved under various device conditions which has been averaged for all dye sizes run and all pressures tested within the devices under equal pressure conditions. From the figure it is observed that a large degree of transport occurs when no cells are present within the devices, as expected. Subsequent addition of an EC

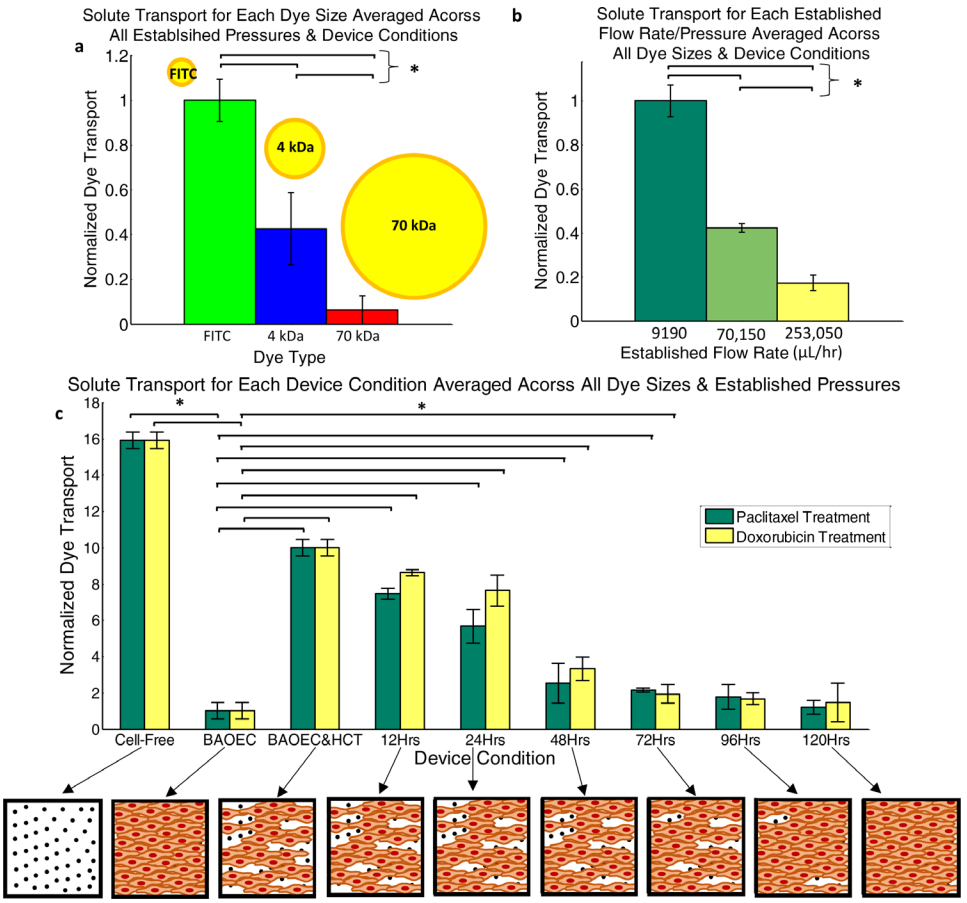

FIG. 3. Averaged and normalized dye transport based on the solute size, established pressure, and device condition for equal pressure tests. Data shown as sum of means ± S.D. (n = 15 independent microfluidic devices) for each image collection method. (a) Overall degree of dye transport based on the dye size, averaged over all established channel pressures, and device conditions tested. Statistical significance of $p < 0.05$ indicated by *. (b) Overall degree of dye transport based on established channel flow rates, averaged over all dye sizes, and device conditions tested. Statistical significance of $p < 0.05$ indicated by *. (c) Overall degree of dye transport based on the device condition, averaged over all dye sizes and established channel pressures tested. Statistical significance of $p < 0.05$ indicated by *. Scheme of typical device conditions depicted for each step of the time-course treatment data.

monolayer resulted in a drastic reduction of overall transport regardless of dye size. Later addition of cancer cells into the basal channel of the devices resulted in an increase in overall transport on average by a factor of around 6. After the addition of cancer cells, treatment with either paclitaxel or doxorubicin over the course of 120 h showed a slow drop in the amount of total transport. After a full 120 h of treatment, the observed dye transport was reduced to conditions experienced with a confluent monolayer of ECs prior to the introduction of cancerous cells. Figure 3(c) contains a representative schema for each condition of the devices throughout the establishment of an EC monolayer, establishment of a cancerous region, and subsequent time-course treatment with therapeutics. It should be noted for Fig. 3(c) that no statistically significant difference existed between the overall transport observed during the time-course treatments with paclitaxel and doxorubicin.

Lastly, it should be noted that cell-free device conditions without cells were run in order to verify that the resistance of the membrane incorperated into the microfluidic system was in the same order of magnitude as values reported in literature for *in vivo* tumors,[27–30] and to function as benchmark testing cases. Additionally, breakdowns of specific data for before averages were calculated across features such as dye size, pressure, or device condition can be seen in the supplementary material, Figs. SF7–SF 9.

III. DISCUSSION

From this work, a platform for studying transport phenomenon in a bi-layer microfluidic device is offered which allows for co-culturing of a variety of cell types. The overall goal of the study was to demonstrate the influences of factors, such as the presence of cancerous cells and established pressures, on the transport of dyes and therapeutic agents in a mimicked blood vessel. The system has also been shown to allow for physiologically relevant flow in the apical channel mimicking microvasculature blood flow and shear. While some portions of the system are held to physiologically relevant conditions, there are several features which are tested over wider ranges for the sake of testing the systems capabilities. The total range, magnitude, and method of generating oncotic pressure in this work are examples of conditions not strictly held to physiologically relevant values. Studying the responsiveness of the system over a wider range of values provided verification that the system is capable of being applied to different disease conditions beyond the scope of cancer microenvironments. Additionally, the unrealistic approach of controlling pressure differences between channels via shear flow allows for more precise regulation when compared to physiological oncotic pressure controlled mainly by protein concentration gradients,[19,22,24] while also providing a means of maintaining a constant therapeutic flux. The use of bovine endothelial cells as opposed to human derived endothelial cells in this work introduces the possibility of variations in the observed results stemming from inter-species differences in EC responses to human cancer cell cytokines, inflammatory agents, antibody interactions, and therapeutic agents.[31–33] In order to facilitate more reliable data collection, future uses of the developed microfluidic system will incorporate the use of human derived endothelial cells such as human umbilical vein endothelial cells (HUVECs). Facilitating the future growth of human derived endothelial cells will require improvements to our microfluidic device performance and functionality in order to ensure that healthy and confluent cultures of human endothelial cells can be grown. As a final note, the use of a semi-permeable membrane within the bi-layer microfluidic model also introduces a physical barrier which is not found *in vivo* and as such introduces an added resistance to the transport of dye and therapeutic molecules. Ideally, such a microfluidic model would be capable of growing a self-supported tubular vessel comprised of human derived endothelial cells, in turn preventing any added resistance to the transport of materials across the device. As such, it should be noted that the observed permeability measurements are lower than what would be expected *in vivo*. This occurs because transport within the boundary of any gaps formed between endothelial cells should occur in an unrestricted manner however, the presence of the semi-permeable membrane restricts the total free area in the cell monolayer gap resulting in a higher resistance and overall reduced transport. Future improvements of the techniques utilized to produce microvasculature within the bi-layer microfluidic system will allow for these issues to be resolved in order to better mimic conditions experienced *in vivo*.

The microfluidic system has been shown to allow for the monitoring of EC permeability and confluency which can be varied based on conditions established within the system. Use of serum-conditioned culture media as opposed to whole blood facilitated ease of use related to data collection and imaging without interference of blood cells, while still providing many of the proteins and small molecule components found in blood plasma. Specifically, the ability to quantify EC monolayer coverage when isolated, exposed to cancerous cells, and throughout the anti-cancer treatment process has been demonstrated. EC coverage was shown to be maximized when only ECs were grown within the apical channel covering nearly 100% of the entire channel. However, upon introduction of HCT116s, the EC coverage dropped to around 65% coverage. The initial EC coverage near 100% was achieved because no cytokines or permeabilizing agents were present within the devices. Later introduction of HCT116s into the basal channels resulted in the release of cytokines and permeabilizing agents into the system. As such, the diffusion and transport of the cytokines/permeabilizing agents to the apical channel resulted in a high degree of EC permeability. Subsequent treatment of the system with either paclitaxel or doxorubicin over 120 h resulted in the slow recovery of the EC coverage back to conditions of nearly 100% coverage. Treatment with either anti-cancer drug, assisted in the recovery of EC

confluency by functioning to kill off the HCT116s growing within the system. As HCT116s were killed off by therapeutics, the production and excretion of cytokines/permeabilizing agents was reduced in turn allowing for EC recovery. It should be noted that the usage of endothelial cells within the microfluidic system was carried out in the form of cell monolayers as opposed to tubular structures. The subsequent use of EC monolayers in turn is recognized to have the potential to influence the performance of the system by altering the regulation of cell-cell and cell-matrix adhesion characteristics based on matrix dimensionality (2D vs. 3D).[34] In addition, it is recognized that the use of endothelial cell monolayers, limits the functionality of the microfluidic system due to the rapid loss of tissue-related functions which impairs the predictive capabilities of the system as a whole.[35] The use of a three dimensional growth system to form endothelial tubes is preferred in order to better mimic EC responses to permeabilizing agents and shear while ensuring that no impairment of the systems predictive capabilities occurs. As such three dimensional tissue growth of endothelial cells into tubular structures will be adopted for future studies involving studies of vasculature.

In addition to observing the influence of the therapeutics on the cancer cells, flow tests were run in devices containing only ECs using therapeutic conditioned media. The resulting data showed initial increases in EC cell counts and confluency over the first 24 h. Continued treatment showed slight decreases in cell counts and confluency as a result of the therapeutics presence. The exposure of ECs to therapeutics slowed their normal growth as apparent when comparing the growth curves of cells treated with standard media and those treated with therapeutic conditions media as seen in the supplementary material, Fig. SF 6. The slow of EC growth and slight reduction in cell counts agrees well with previous findings in literature and is known to occur as a result of the manner in which the two therapeutics function to cause cell death.[36–39] In addition, only slight variations in EC confluency were noted as a result of being exposed to the therapeutics. The variations which were observed can be contributed to the combination of fluctuations in cell counts and changes in the EC morphology. The scale of fluctuation in EC permeability resulting from the therapeutics alone was relatively low when compared to the fluctuations observed when cancer cells were present in the system. As such, the major focus of the work was geared around permeability induced by the presence of the HCT116 cancer cells. Overall, this work has shown that the system is able to function as a suitable method for observing cellular scale changes in EC confluency and permeability resulting from the presence of cancer cells and anti-cancer therapeutics. It should be noted that measurements of EC permeability were carried out with direct cell imaging measurements and indirectly via dye transport studies. The observed gaps which formed between ECs as a result of being exposed to cancerous cytokines and permeabilizing agents are what facilitated the apical to basal transport of the dyes used. The presence of a semi-permeable membrane in the microfluidic system was required to function as a physical substrate onto which ECs could anchor, which also serves to introduce a small amount of resistance to fully unrestricted dye transport. However, decisions on the pore size and density for the membranes were chosen to reduce the unavoidable transport resistance as much as possible. As such, this study focuses on quantifying the influence of factors such as cytokines/permeabilizing agents (resulting from cancerous disease conditions), pressure differentials, and shear flow on the observed permeability of the vascular endothelium to variously sized dye molecules. Beyond the scope of monitoring EC monolayer integrity, the system was shown to be capable of performing therapeutic/tracer delivery studies which will be discussed next.

Leveraging the ability to dictate precise pressures within both channels of the devices, a variety of equal pressure cases were tested to observe the effect of pressure/flow rate on therapeutic delivery. Given that the pressures established in each channel can be controlled independently, we chose to investigate the effects of various equal pressure test cases on therapeutic transport. In addition to the use of equal pressures, a range of dye sizes and device conditions were established in order to further understand how transport if influenced.

When considering the influence of solute size on transport, the maximum amount of transport observed occurred for FITC, followed by FITC-Dextran 4 kDa, and FITC-Dextran 70 kDa, respectively. This trend in transport is observed due to the dye molecules various sizes. The

smallest FITC dye underwent the greatest transport because it is more freely able to diffuse through the system. The larger dyes take longer times to diffuse around in the system and as such, they undergo less transport over the same time-period. The large influence of the dye size on the observed transport is credited to the fact that under equal pressure conditions, the main factors driving transport are the natural diffusion of the dyes and the concentration gradients which exist across the semi-permeable membrane. Since size plays a large role in dye diffusion, a large difference in transport is observed between the three dyes. In addition to dye size, the established pressures within the channels also largely influence transport.

The wide range of equal pressures tested resulted in differing degrees of transport. Given the resulting transport trend, it was observed that increasing the pressure within the system while still maintaining equal pressures on both halves of the device, resulted in reduced transport of dyes regardless of size. This trend was observed due to the fact that the total volume of dye suspension introduced into each device was held constant. As such, the increased pressures being generated by increased flow rates resulted in less time for the dye molecules to diffuse while in the system. If the duration of flow for each pressure case was held constant instead of the total volume, then no difference in transport between established channel pressures would be expected, as verified via cell-free device testing data in the supplementary material, Fig. SF 10. Moving beyond the scope of established channel pressures, studies were conducted to identify the influence of system conditions on the transport of therapeutics.

From this section of the study, a range of system conditions were established including cell-free, EC confluent, EC and HCT116 diseased devices and the subsequent application of time-course therapeutic treatments. The greatest degree of dye transport was observed under device conditions containing no cells (cell-free) which agreed well with the predicted theoretical model based on the Kedem-Katchalsky transport equations[40] [see the supplementary material, Fig. SF 7(a)]. Later establishment of an EC monolayer within the apical channel resulted in greatly reduced transport due to the formation of a confluent monolayer. The overall transport was reduced due to coverage of the pores present in the semi-permeable membrane by the ECs. Instead of being able to transport across the semi-permeable membrane, the dyes introduced into the apical channel were forced to exit the system from the apical channel outlet. These observed results agree well with trends published in similar studies utilizing the microfluidic system to study endothelial permeability to tumor cells.[41]

Further addition of HCT116s resulted in the partial recovery of transport within the system. The observed partial transport recovery is the result of cytokines and permeabilizing agents, released by the newly added HCT116s, functioning to permeabilize the EC monolayer. The formation of large gaps between ECs in the apical channel allowed for the exposure of pores in the membrane which in turn allowed for increased dye and therapeutic transport. Again, the observed results agree with previous literature findings using metastatic cancer cell lines, tumor conditioned media containing excreted cytokines/permeabilizing agents, and similar dye molecules.[41] Moving beyond the diseased state of the system, the application of anti-cancer therapeutics was investigated in order to verify that the system as a whole responds to the presence of therapeutic agents.

Paclitaxel and Doxorubicin were utilized to treat the cancerous regions of the devices in order to observe the recovery process of the EC monolayers. Subsequent treatment of the system with either of the therapeutics over the course of 120 h resulted in the recovery of the EC monolayers as measured directly with imaging (see Fig. 2) and indirectly via dye transport measurements. The observed increase in cancerous cell death upon treatment with either paclitaxel or doxorubicin agrees with other literature studies.[42–45] Additionally, the observed reduction in EC permeability during treatment with either of the anti-cancer therapeutics agrees with trends observed in literature.[5,46–48] Time-course treatments were only run over the course of 120 h because the EC permeability and dye transport were able to recover back to conditions similar to those experienced prior to the introduction of cancerous cells. Additionally, there exist other *in vivo* based tumor studies which have been run over the course of five to seven days, making the choice of 120 h of treatment in our model suitable.[11,49–51]

Introduction of therapeutics into the apical channel along with dye molecules was performed in order to observe if the amount of transported dye would be influenced by the treatment of the diseased cancerous environment. Transport of the anti-cancer therapeutics across the membrane functioned to slowly kill off the HCT116s present in the basal channel of the devices. In turn the death of HCTs reduced the amount and degree of cytokine/permeabilizing agent secretion. The EC monolayers were shown to recover over the 120 h treatment process as a result of HCT116 cell death. These results confirmed that the system was functioning to facilitate therapeutic transport across the EC monolayer and semi-permeable membrane. The observed changes in dye transport resulting from therapeutic treatment serve as an indirect technique for quantitatively analyzing the degree of EC permeability. Additionally, an understanding of how therapeutic treatments influence cancerous and endothelial cells can be gained through the use of the developed microfluidic system. As noted previously, the direct influence of the therapeutics on EC permeability have been quantified and should be given consideration when choosing potential anti-cancer therapeutic treatments for patients.

Overall, the developed microfluidic system has been shown to allow for the establishment of EC monolayers which are responsive to their local environment while also facilitating physiologically relevant flows in the apical channel. The additional ability to grow secondary cell types, such as cancerous cells, in close proximity to the mimicked blood vessel provides the opportunity to study interactions and responses between the chosen cell types. Further, the ability to precisely control and regulate pressures within each channel provides opportunities to study various disease conditions such as tumor microenvironments. In this work, we have utilized endothelial and tumor cells to establish a simplified tumor microenvironment in order to study endothelial responses to cancerous cells/anti-cancer therapeutics, the therapeutic delivery process in a mimicked vessel, and the responsiveness of HCT116 cells to treatment with paclitaxel and doxorubicin. It should be noted that this approach does not consider all conditions experienced in an *in vivo* tumor microenvironment. Furthermore, it is noted that certain parameters and conditions established within the system do not always fall within physiologically relevant ranges. The use of values outside of physiologically relevant ranges is performed for the sake of testing the system's functionality for potential work outside the scope of mimicking tumor microenvironments. Future applications of this technology towards early stage testing of personalized therapeutic options has the potential of utilizing patient derived cells as a means of improving the delivery and effectiveness of therapeutic systems. Future work for the system is being focused on improving functionality for improved testing. Some specific improvements include the establishment of a more diversified set of applications for additional disease models (inflammation and gastrointestinal drug delivery), establishment of culturing procedures to provide a wider range of cell types to be used, and introduction of a 3D environment for growth of tumor spheroids as opposed to monolayers of cancer cells as utilized in the current work.

IV. METHODS

A. Device fabrication

Microfluidic devices were fabricated using polydimethylsiloxane (PDMS) (SYLGARD 184, Dow Corning) and assembled into a bi-layer device as depicted in Fig. 1. The devices were fabricated using two separate pieces of PDMS with channels molded into them and a polycarbonate semi-permeable membrane (Whatman Cyclopore, Sigma-Aldrich). The semi-permeable membrane is adhered to both pieces of PDMS and sandwiched between the overlapping regions of the channels. The regions where the channels in both pieces of PDMS overlap facilitate transport from one channel into the other through the pores in the semi-permeable membrane. As a result, the pores of the membrane act to dictate the maximum size of materials which can be transferred. In order to only allow for culturing media and small chemical components to pass from one channel to the other while restricting the transport of cells, a membrane with an average pore size of one micrometer was chosen. Because cells are not capable of passing through the membrane, a co-culture setup is achievable by growing bovine aortic endothelial cells (BAOECs) on the top surface of the membrane within the apical channel, while human

colorectal cancer cells (HCT116s) are grown on the bottom surface of the lower channel termed the basal channel as depicted in the supplementary material, Fig. SF 1.

B. Cell growth on device

After fabrication of the microfluidic devices, both the apical and basal channels were filled with a 0.5% porcine gelatin (PG) (0.5%, Sigma-Aldrich) solution and incubated for 30 min at 37 °C and 5% CO_2. After incubation, the PG was removed and replaced with BAOEC (Cell Applications, San Diego, CA) suspension in the apical channel and incubated for 12 h to allow for cell adhesion to the top side of the semi-permeable membrane. After 12 h, all remaining cell suspension was washed away by establishing media [DMEM(1×) + GlutaMAX – I (gibco, life technologies), 10% HI-FBS (Sigma-Aldrich), 1% Penn/Strep Antibiotic(1×) (Gibco, life Technologies)] flow within the channel using sterile tubing, syringe and syringe pump (PHD 2000, Harvard Apparatus). The flow rate established within the channel was kept low for purposes of media exchange and aligning the BAOECs to flow. These flow based incubation conditions were held constant typically for 3 to 4 days until the endothelial monolayer on the semi-permeable membrane reached confluency. Upon achieving a confluent BAOEC monolayer in the apical channel, HCT116s (ATCC, Manassas, VA) were introduced into the basal channel and allowed to settle and adhere to the bottom of the basal channel for 24 to 48 h. HCT116 cells were introduced into the devices in order to permeabilize BAOEC monolayers similar to conditions found in various cancerous disease states. Once the HCT116 cells properly adhered, a flow rate equivalent to that established in the apical channel was setup in the basal channel using a secondary syringe pump. Both the BAOEC and HCT116 cells were grown within the bi-layer device under these flow conditions within an incubator until experimental proceedings began.

C. Establishing shear rate

The effect of fluid shear on the growth of cells and transport of compounds from channel to channel is established using syringe pumps (PHD 2000, Harvard Apparatus). The syringe pumps allow for control over the flow rates established in both channels of the device. By altering the flow rate within the channels, we are able to specifically set and control the shear rate imparted on the cells growing within each channel and any other materials introduced into the channel along with the flowing media. The equation governing[52] the shear rate established in each of the channels is as follows: $Shear\,Rate = \left(\frac{6Q}{W*H^2}\right)\left(1+\frac{H}{W}\right)(f^*)\left(\frac{H}{W}\right)$, where Q is the established flow rate within the given channel, W is the channel width, H is the channel height, and f^* is a geometrical factor based on channel dimensions which for the microfluidic devices used is 0.7946. The width and height dimensions for the channels utilized in this study were 500 μm and 100 μm, respectively. In order to stay within a physiologically relevant range,[53–55] the shear rate in the apical channel containing the BAOECs was held at 200 s^{-1} which is at the lower end of range typically experienced within the arterioles of the body. The shear rate established within the basal channel containing HCT116s was held constant with the shear in the apical channel to prevent any convective flux between channels when not desired. While initially culturing cells within both channels, the shear rate was typically set around 50 s^{-1} as a means of simply refreshing media exposed to the cells for continued growth while not imparting drastically high shear. It should be noted that both equal and differing shear rates were established in the channels depending on if a pressure difference across the semi-permeable membrane was desired.

D. Establishing pressures within the channels

In order to simulate the effect of pressures within the system, the relative shear rates established in the channels were varied to achieve desired average channel pressures. In order to prevent the establishment of a pressure differential across the semi-permeable membrane, the shear rates established in both the apical and basal channel were maintained at equal values. The

governing equation[56] used to relate the established shear rates in each channel with the average pressure difference across the membrane is as follows:

$$P_{\Delta} = \frac{\frac{12\mu_1 L_1 Q_1}{W_1 H_1^3}}{\frac{1 - \left(\frac{192H_1}{\pi^5 W_1}\right)\left(\tanh\left(\frac{\pi W_1}{2H_1}\right)\right)}{2}} - \frac{\frac{12\mu_2 L_2 Q_2}{W_2 H_2^3}}{\frac{1 - \left(\frac{192H_2}{\pi^5 W_2}\right)\left(\tanh\left(\frac{\pi W_2}{2H_2}\right)\right)}{2}},$$

where μ_1 and μ_2 are the viscosity of the fluid in the apical and basal channels respectively, L_1 and L_2 are the overall length of the apical and basal channel respectively, Q_1 and Q_2 are the flow rates established in the apical and basal channels respectively, W_1 and W_2 are the widths of the apical and basal channels, and H_1 and H_2 are the heights of the apical and basal channels, respectively. The above equation calculates the average pressure generated in the apical channel and subtracts from it, the average pressure generated in the basal channel. In this case, when P_{Δ} is equal to zero, it indicates that the average pressures in both the apical and basal channels are the same, allowing for the determination of the flow rates required to achieve the balance of apical and basal channel pressures.

E. Cell imaging and confluency measurements

Cells grown on devices were imaged utilizing standard fluorescence imaging microscopy (Olympus IX70, Hamamatsu C9300, Plan Fluor 10× and 20×, NA: 0.3, RI: 1). For fluorescence imaging, the plasma membranes of the cultured cells were stained with Cell Tracker Green™ (10 μM, Thermo Fisher Scientific) plasma membrane stain to identify the outer most boundaries of the cells occupying the culturing area. This method of cell plasma membrane (PM) staining allows for the quantification of the area specifically covered by cells within the viewing area of the various fluorescence microscopes. Images taken via conventional fluorescence microscopy were utilized to determine the overall cellular monolayer confluency. These measurements were carried out using the FIGI (ImageJ) software suite[57,58] and the collected image. The imaging technique was used to obtain the average degree of monolayer confluency as well as to quantify the area occupied by gaps between cells. The analysis for the cell coverage measurements was taken once the cells had reached confluency within the apical channel of the device just before HCT116s were introduced into the basal channel. A second measurement of all devices was taken at 24 to 48 h after introduction of HCT116s into the basal channel. Lastly, final measurements for each device were taken 12, 24, 48, 72, 96, and 120 h after introduction of anti-cancer therapeutics into the device. The image acquisition software utilized includes HCImage Live (Hamamatsu Photonics) for standard fluorescence imaging and NIS-Elements (Nikon) for acquisition of confocal images.

F. Anti-cancer therapeutics

In order to study how particle transport is influenced by variations in the endothelial monolayer permeability, BAOECs were exposed to HCT116s. Treatment of the microfluidic system with the anti-cancer therapeutics, Paclitaxel and Doxorubicin, allowed for varying degrees of BAOEC permeability within the diseased state setup. The working concentrations for both Paclitaxel and Doxorubicin were 5 ng/ml for all experimental testing. Paclitaxel and Doxorubicin functioned to eliminate cancer cells and were chosen due to their wide use, high degree of documentation for *in vitro* and *in vivo* data, and relatively inexpensive cost. The anti-cancer therapeutics were introduced into the apical channel of the devices in order to mimic an intravenous administration. For time-course studies, the anti-cancer therapeutics were continuously introduced into the system via the apical channel over the entire course of 120 h. Any therapeutic introduced into the microfluidic system was subjected to the shear established within the device in order to mimic the situation or blood flow within the body. Therapeutics which successfully transitioned from the apical channel through the semi-permeable membrane into the basal channel were able to act on the HCT116s present. Interaction of the anti-cancer

drugs with the HCT116s resulted in the death of affected cells, which in turn were washed away downstream and eventually out of the device into the waste media collection containers. As such, the HCT116 cells which were killed off and washed away could no longer contribute to the secretion of permeabilizing agents. Lastly, in order to ensure that the presence of the anti-cancer therapeutics caused HCT116 cell death, microfluidic devices containing only HCT116s were subjected to either of the two therapeutics, with cell death verified via cell staining and fluorescence microscopy before and after treatment, as seen in the supplementary material, Fig. SF 11. Chemical authentication and validation data for the Paclitaxel and Doxorubicin utilized in this work were provided by LC Laboratories (Paclitaxel—Prod. No.: P-9600 Lot: ASM-118; Doxorubicin—Prod. No.: D-4000 Lot: DXR-110).

Interaction of the anti-cancer therapeutics with BAOECs and subsequent EC cellular responses were investigated by establishing endothelial monolayers within the microfluidic devices without the presence of any cancer cells. Therapeutic solutions were prepared at the same concentrations as described previously. Therapeutic conditioned media was flown through the devices and the BAOECs were stained with Cell Tracker Green in order to facilitate fluorescent imaging. Therapeutic solution flows were established for 120 h with cell images collected every 24 h. The resulting images were collected for cell count and EC monolayer permeability measurements. Relative comparisons were made between values measured prior to therapeutic flows (0 h) and all other measured time points.

G. Dye cross-vasculature equal pressure transport studies

Dye transport was achieved by flowing dye into the bi-layer channel via a syringe pump. In order to quantify the degree of transport for each test case, the outlet flow of both the apical and basal channels was collected separately and distributed into well plates. The fluorescence intensities of the flow-through were measured via a plate reader with excitation at 490 nm and emission read at 525 nm. The dyes utilized in the study include FITC at a working concentration of 0.625 mg/ml, FITC-Dextran 4 kDa at a working concentration of 5 mg/ml, and FITC-Dextran 70 kDa at a working concentration of 5 mg/ml. The working concentrations for each dye were chosen so that a sufficient fluorescence intensity signal was obtained from the experimental testing for measurement purposes. The basal outlet contained dye which successfully transported across the semi-permeable membrane, and dye exiting out of the apical outlet was collected and measured to ensure that the total dye concentration introduced into the devices was accounted for at both the outlets.

The transport studies were carried out under three device conditions as follows, cell-free devices, devices with only a BAOEC confluent monolayer, and diseased devices containing a monolayer of BAOECs in the apical channel, and a monolayer of HCT116s in the basal channel which were then subjected to a time-course therapeutic treatment. The second and third device conditions established allowed for studies on the ability of dyes to transport under varying degrees of BAOEC permeability. All rounds of transport studies were carried out with flow established in the apical and basal channels. In order to mimic the various pressure conditions experienced within the vasculature, the first rounds of testing were carried out so that no pressure difference was established across the semi-permeable membrane. The pressures established in both the apical and basal channels for these studies were 632.8, 4832.4, and 17431.2 Pa, which were established in addition to the physiologically normal pressure of 10 666 Pa (80 mm Hg). Cell-free device studies did not utilize any cell culturing within the channels prior to introduction of particle suspensions. Devices run with BAOEC confluent monolayers were established 3 to 4 days prior to dye flows to ensure that a highly confluent monolayer was present in the apical channel over the semi-permeable membrane. Lastly, the diseased state devices were prepared 6 to 8 days in advance of dye flows. 3 to 4 days were spent growing a confluent apical BAOEC monolayer and the remaining days were spent producing a cancer cell monolayer in the basal channel. The transport studies were carried out under adjusted timeframes to ensure that the same amount of dye introduced into each device was the same regardless of the pressure being used. One final note for the diseased state devices was the later introduction of an

anti-cancer therapeutic to influence the cancer cells in the basal channel and the confluency of the BAOEC monolayer in the apical channel. The degree of dye transport was documented throughout a time-course treatment with Paclitaxel and Doxorubicin to understand how the BAOEC monolayer integrity influenced the dye transport capabilities. Experimental schemes for this testing can be observed in the supplementary material, Figs. SF 1 and SF 2.

H. Statistical analysis

Statistical analysis of all the obtained results was run utilizing IBM's SPSS statistical software package (IBM Corp.). All of the figures have significant differences indicated above elements within the plots. One way analysis of variance (one-way ANOVA) tests were run for each data set with confidence levels of 95% held throughout all plots. All analyses were carried out under conditions of Tukey equal variances assumed, along with tests of homogeneity of variance further verified by both Brown-Forsythe and Welch analyses. Based on the obtained statistical results, all bar graphs contain grouped pairs between groups and within groups indicating statistically significant differences between means indicated by "*." For all line plots, statistically significant differences in means are compared against the baseline tests for the spherically shaped particles. Significance between both the short rod particle and long rod particle values are indicated by "*." Significant differences between means for short rod and long rod particles are indicated by "**," noting that all differences are given at a confidence level of 95%. Within group F values and degrees of freedom for each plot are noted in their respective legends. Sample sizes for all experimental testing were determined by performing estimation for multiple-sample one-way ANOVA pairwise comparison based on pilot studies utilizing the standard sample size approximation of: $n_{ij} = \frac{2(z_{\frac{\alpha}{2}}+z_{\beta})^2\sigma^2}{\epsilon_{ij}^2}$. All statistical comparisons are run under assumptions of equal variance between groups. This assumption is verified via the Levene's Test, where all *p values* must be greater than 0.05 in order to verify the equal variance assumption across groups. All data sets presented in this work pass the Levene's Test with *p values* greater than 0.05.

I. Data availability

The datasets generated during and/or analyzed during the current study are available from the corresponding author upon reasonable request.

J. Cell line authentication

The cell lines utilized in this work do not appear on the "List of Commonly Misidentified Cell Lines" maintained by the International Cell Line Authentication Committee (ICLAC). Cell line authentications (BAOEC: Cell Applications B304-05 and HCT116: ATCC CCL-247) have been provided directly from cell line source. Mycoplasma tests were negative for both cell types used via the fluorescence mycoplasma detection kit (MycoFluor Mycoplasma Detection Kit, Sigma-Aldrich, M7006).

SUPPLEMENTARY MATERIAL

See supplementary material for experimental schemes along with supporting figures of data and representative images collected throughout the experimental work. Figures include data regarding time-course measurements of cell confluency and dye transport under various experimental conditions.

ACKNOWLEDGMENTS

This work is partially supported by the National Science Foundation (Grant NSF IIP-1701136, CBET-1113040, CBET-1067502, DMS-1516236 to YL), the National Institutes of Health (NIH) (Grant R01HL131750 and EB015105 to YL), the Pennsylvania Infrastructure Technology Alliance (PITA) program and the Alternatives Research & Development Foundation.

[1]B. P. Eliceiri, R. Paul, P. L. Schwartzberg, J. D. Hood, J. Leng, and D. A. Cheresh, "Selective requirement for Src kinases during VEGF-induced angiogenesis and vascular permeability," Mol. Cell. **4**(6), 915–924 (1999).
[2]S. Shresta, K. L. Sharar, D. M. Prigozhin, P. R. Beatty, and E. Harris, "Murine model for dengue virus-induced lethal disease with increased vascular permeability," J. Virol. **80**(20), 10208–10217 (2006).
[3]H. Maeda, J. Wu, T. Sawa, Y. Matsumura, and K. Hori, "Tumor vascular permeability and the EPR effect in macromolecular therapeutics: A review," J. Controlled Release **65**(1–2), 271–284 (2000).
[4]S. M. Weis and D. A. Cheresh, "Pathophysiological consequences of VEGF-induced vascular permeability," Nature. **437**(7058), 497–504 (2005).
[5]D. R. Senger, S. J. Galli, A. M. Dvorak, C. A. Perruzzi, V. S. Harvey, and H. F. Dvorak, "Tumor cells secrete a vascular permeability factor that promotes accumulation of ascites fluid," Science **219**(4587), 983–985 (1983).
[6]H. Maeda, J. Fang, T. Inutsuka, and Y. Kitamoto, "Vascular permeability enhancement in solid tumor: Various factors, mechanisms involved and its implications," Int. Immunopharmacol. **3**, 319–328 (2003).
[7]A. K. Iyer, G. Khaled, J. Fang, and H. Maeda, "Exploiting the enhanced permeability and retention effect for tumor targeting," Drug Discov. Today **11**(17–18), 812–818 (2006).
[8]R. K. Jain, "Normalization of tumor vasculature: An emerging concept in antiangiogenic therapy," Science **307**(5706), 58–62 (2005).
[9]V. Torchilin, "Tumor delivery of macromolecular drugs based on the EPR effect," Adv. Drug Delivery Rev. **63**(3), 131–135 (2011).
[10]J. Fang, H. Nakamura, and H. Maeda, "The EPR effect: Unique features of tumor blood vessels for drug delivery, factors involved, and limitations and augmentation of the effect," Adv. Drug Delivery Rev. **63**(3), 136–151 (2011).
[11]H. Maeda, G. Y. Bharate, and J. Daruwalla, "Polymeric drugs for efficient tumor-targeted drug delivery based on EPR-effect," Eur. J. Pharm. Biopharm. **71**(3), 409–419 (2009).
[12]R. Singh and J. W. Lillard, "Nanoparticle-based targeted drug delivery," Exp. Mol. Pathol. **86**(3), 215–223 (2009).
[13]Y. H. Bae and K. Park, "Targeted drug delivery to tumors: Myths, reality and possibility," J. Controlled Release **153**(3), 198–205 (2011).
[14]J. M. Brown and A. J. Giaccia, "The unique physiology of solid tumors: Opportunities (and problems) for cancer therapy," Cancer Res. **58**(7), 1408–1416 (1998).
[15]S. K. Sriraman, B. Aryasomayajula, and V. P. Torchilin, "Barriers to drug delivery in solid tumors," Tissue Barriers. **2**, e29528 (2014).
[16]T. T. Batchelor, A. G. Sorensen, E. di Tomaso *et al.*, "AZD2171, a Pan-VEGF receptor tyrosine kinase inhibitor, normalizes tumor vasculature and alleviates edema in glioblastoma patients," Cancer Cell **11**(1), 83–95 (2007).
[17]M. R. Mancuso, R. Davis, S. M. Norberg *et al.*, "Rapid vascular regrowth in tumors after reversal of VEGF inhibition," J. Clin. Invest. **116**(10), 2610–2621 (2006).
[18]K. J. Heyeraas and E. Berggreen, "Interstitial fluid pressure in normal and inflamed pulp," Crit. Rev. Oral Biol. Med. **10**(3), 328–336 (1999).
[19]C.-H. Heldin, K. Rubin, K. Pietras, and A. Ostman, "High interstitial fluid pressure - An obstacle in cancer therapy," Nat. Rev. Cancer **4**(10), 806–813 (2004).
[20]A. Thomas, H. Daniel Ou-Yang, L. Lowe-Krentz, V. R. Muzykantov, and Y. Liu, "Biomimetic channel modeling local vascular dynamics of pro-inflammatory endothelial changes," Biomicrofluidics **10**(1), 014101 (2016).
[21]A. Thomas, S. Wang, S. Sohrabi *et al.*, "Characterization of vascular permeability using a biomimetic microfluidic blood vessel model," Biomicrofluidics. **11**(2), 024102 (2017).
[22]H. F. Dvorak, "Vascular permeability factor/vascular endothelial growth factor: A critical cytokine in tumor angiogenesis and a potential target for diagnosis and therapy," J. Clin. Oncol. **20**(21), 4368–4380 (2002).
[23]D. R. Senger, L. Van De Water, L. F. Brown *et al.*, "Vascular permeability factor (VPF, VEGF) in tumor biology," Cancer Metastasis Rev. **12**(3–4), 303–324 (1993).
[24]J. A. Nagy, A. M. Dvorak, and H. F. Dvorak, "Vascular hyperpermeability, angiogenesis, and stroma generation," Cold Spring Harbor Perspect. Med. **2**(2), a006544 (2012).
[25]R. Green, E. E. Windhage, and G. Giebisch, "Protein oncotic pressure effects on proximal tubular fluid movement in rat," Am. J. Physiol. **226**(2), 265–276 (1974).
[26]M. Stohrer, Y. Boucher, M. Stangassinger, and R. K. Jain, "Oncotic pressure in solid tumors is elevated," Cancer Res. **60**(15), 4251–4255 (2000).
[27]E. S. Marie, R. K. Jain, and E. M. Sevick, "Effect of red blood cell rigidity on tumor blood flow: Increase in viscous resistance during hyperglycemia," Cancer Res. **51**(10), 2727–2730 (1991).
[28]R. P. McCall and M. Sher, "The physics of the human body," Am. J. Phys. **80**(2), 174 (2012).
[29]K. H. Jensen, A. X. C. N. Valente, and H. A. Stone, "Flow rate through microfilters: Influence of the pore size distribution, hydrodynamic interactions, wall slip, and inertia," Phys. Fluids **26**(5), 52004 (2014).
[30]R. K. Jain, "Determinants of tumor blood flow: A review," Cancer Res. **48**(10), 2641–2658 (1988).
[31]M. W. Radomski, R. M. Palmer, and S. Moncada, "Endogenous nitric oxide inhibits human platelet adhesion to vascular endothelium," Lancet **330**(8567), 1057–1058 (1987).
[32]R. J. Ober, C. G. Radu, V. Ghetie, and E. S. Ward, "Differences in promiscuity for antibody-FcRn interactions across species: Implications for therapeutic antibodies," Int. Immunol. **13**(12), 1551–1559 (2001).
[33]J. Folkman, C. C. Haudenschild, and B. R. Zetter, "Long-term culture of capillary endothelial cells," Proc. Natl. Acad. Sci. U.S.A. **76**(10), 5217–5221 (1979).
[34]F. J. Byfield, R. K. Reen, T. P. Shentu, I. Levitan, and K. J. Gooch, "Endothelial actin and cell stiffness is modulated by substrate stiffness in 2D and 3D," J. Biomech. **42**(8), 1114–1119 (2009).
[35]F. Pampaloni, E. G. Reynaud, and E. H. K. Stelzer, "The third dimension bridges the gap between cell culture and live tissue," Nat. Rev. Mol. Cell Biol. **8**(10), 839–845 (2007).
[36]M. Muta, T. Yanagawa, Y. Sai *et al.*, "Effect of low-dose paclitaxel and docetaxel on endothelial progenitor cells," Oncology **77**(3–4), 182–191 (2009).
[37]E. Pasquier, S. Honore, B. Pourroy *et al.*, "Antiangiogenic concentrations of paclitaxel induce an increase in microtubule dynamics in endothelial cells but not in cancer cells," Cancer Res. **65**(6), 2433–2440 (2005).

[38]J. Folkman, "Angiogenesis and apoptosis," Semin. Cancer Biol. **13**(2), 159–167 (2003).
[39]D. S. Grant, T. L. Williams, M. Zahaczewsky, and A. P. Dicker, "Comparison of antiangiogenic activities using paclitaxel (taxol) and docetaxel (taxotere)," Int. J. Cancer **104**(1), 121–129 (2003).
[40]M. Sugihara-Seki and B. M. Fu, "Blood flow and permeability in microvessels," Fluid Dyn. Res. **37**(1–2), 82–132 (2005).
[41]Y. Tang, F. Soroush, J. B. Sheffield, B. Wang, B. Prabhakarpandian, and M. F. Kiani, "A biomimetic microfluidic tumor microenvironment platform mimicking the EPR effect for rapid screening of drug delivery systems," Sci. Rep. **7**, 9359 (2017).
[42]H. D. Bear, S. Anderson, A. Brown *et al*., "The effect on tumor response of adding sequential preoperative docetaxel to preoperative doxorubicin and cyclophosphamide: Preliminary results from National Surgical Adjuvant Breast and Bowel Project Protocol B-27," J. Clin. Oncol. **21**(22), 4165–4174 (2003).
[43]G. Maschek, N. Savaraj, W. Priebe *et al*., "2-Deoxy-D-glucose increases the efficacy of adriamycin and paclitaxel in human osteosarcoma and non-small cell lung cancers in vivo," Cancer Res. **64**(1), 31–34 (2004).
[44]J. Baselga, L. Norton, J. Albanell, Y. M. Kim, and J. Mendelsohn, "Recombinant humanized anti-HER2 antibody (herceptin(TM)) enhances the antitumor activity of paclitaxel and doxorubicin against HER2/neu overexpressing human breast cancer xenografts," Cancer Res. **58**(13), 2825–2831 (1998).
[45]L. Hu, J. Hofmann, Y. Lu, G. B. Mills, and R. B. Jaffe, "Inhibition of phosphatidylinositol 3′-kinase increases efficacy of paclitaxel in in vitro and in vivo ovarian cancer models," Cancer Res. **62**(4), 1087–1092 (2002).
[46]F. Yuan, Y. Chen, M. Dellian, N. Safabakhsh, N. Ferrara, and R. K. Jain, "Time-dependent vascular regression and permeability changes in established human tumor xenografts induced by an anti-vascular endothelial growth factor/vascular permeability factor antibody," Proc. Natl. Acad. Sci. U.S.A. **93**(25), 14765–14770 (1996).
[47]R. T. Tong, Y. Boucher, S. V. Kozin, F. Winkler, D. J. Hicklin, and R. K. Jain, "Vascular normalization by vascular endothelial growth factor receptor 2 blockade induces a pressure gradient across the vasculature and improves drug penetration in tumors," Cancer Res. **64**(11), 3731–3736 (2004).
[48]S. Goel, D. G. Duda, L. Xu *et al*., "Normalization of the vasculature for treatment of cancer and other diseases," Physiol. Rev. **91**(3), 1071–1121 (2011).
[49]H. Walczak, R. E. Miller, K. Ariail *et al*., "Tumoricidal activity of tumor necrosis factor-related apoptosis-inducing ligand in vivo," Nat. Med. **5**(2), 157–163 (1999).
[50]J. P. Stevenson, M. Rosen, W. Sun *et al*., "Phase I trial of the antivascular agent combretastatin A4 phosphate on a 5-day schedule to patients with cancer: Magnetic resonance imaging evidence for altered tumor blood flow," J. Clin. Oncol. **21**(23), 4428–4438 (2003).
[51]T. Fujiwara, E. A. Grimm, T. Mukhopadhyay, W. W. Zhang, L. B. Owen-Schaub, and J. A. Roth, "Induction of chemosensitivity in human lung cancer cells in vivo by adenovirus-mediated transfer of the wild-type p53 gene," Cancer Res. **54**(9), 2287–2291 (1994).
[52]Y. Son, "Determination of shear viscosity and shear rate from pressure drop and flow rate relationship in a rectangular channel," Polymer **48**(2), 632–637 (2007).
[53]P. Nigro, J.-I. Abe, and B. C. Berk, "Flow shear stress and atherosclerosis: A matter of site specificity," Antioxid. Redox Signaling **15**(5), 1405–1414 (2011).
[54]T. Nagaoka and A. Yoshida, "Noninvasive evaluation of wall shear stress on retinal microcirculation in humans," Invest. Ophthalmol. Visual Sci. **47**(3), 1113–1119 (2006).
[55]A. Thomas, J. Tan, and Y. Liu, "Characterization of nanoparticle delivery in microcirculation using a microfluidic device," Microvasc. Res. **94**, 17–27 (2014).
[56]A. Zanella and A. Biral, "Microfluidic networking: Modelling and analysis," dissertation (University of Padua, 2012).
[57]E. C. Jensen, "Quantitative analysis of histological staining and fluorescence using ImageJ," Anat. Rec. **296**(3), 378–381 (2013).
[58]W. Rasband, see https://imagej.nih.gov/ij/ for ImageJ (U.S. National Institutes of Health, Bethesda, Maryland, USA, 2017).